Experimental extraction of neutron resonance parameters at 20-300 eV for ^{147,149}Sm

X.X. Li (李鑫祥),[1,*] L.X. Liu (刘龙祥),[2] W. Jiang (蒋伟),[3,4] Y.J. Chen (陈雅菊),[1] J. Ren (任杰),[5] H.W. Wang (王宏伟),[2,6,†] G.T. Fan (范功涛),[2,6] W. Luo (罗文),[1,‡] S. Feng (冯松),[1] W. Xie (谢文),[1] Z.A. Lin (林子昂),[1] T. Jiang (江婷),[1] G.L. Yang (杨高乐),[7] Z.D. An (安振东),[8] X.K. Li (黎先锴),[1,7] Z.J. Liao (廖周济),[1] J.M. Xue (薛洁明),[9] X.Y. Li (李欣雨),[10] N.X. Peng (彭宁馨),[1] D.X. Wang (王德鑫),[11] S.Y Zhang (张苏雅拉吐),[11] Y. Zhang (张岳),[2] X.R. Hu (胡新荣),[12] Z.R. Hao (郝子锐),[2] B. Jiang (姜炳),[3,4] X.H. Wang (王小鹤),[13] J.F. Hu (胡继峰),[13] Y.D. Liu (刘应都),[14] C.W. Ma (马春旺),[15,16] Y.T. Wang (王玉廷),[15] J.J. He (何建军),[17] and L.Y. Zhang (张立勇)[18,19]

[1]*School of Nuclear Science and Technology, University of South China, Hengyang 421001, China*
[2]*Shanghai Advanced Research Institute, Chinese Academy of Sciences, Shanghai 201210, China*
[3]*Institute of High Energy Physics, Chinese Academy of Sciences, Beijing,100049,China*
[4]*China Spallation Neutron Source, Dongguan, 523803, China*
[5]*China Institute of Atomic Energy, Beijing, 102413, China*
[6]*University of Chinese Academy of Sciences, Beijing 100049, China*
[7]*Sun Yat-sen University, Zhuhai, 510275, China*
[8]*Institute of Modern Physics, Chinese Academy of Sciences, Lanzhou 730000, China*
[9]*Key Laboratory of Nuclear Data, China Institute of Atomic Energy, Beijing 102413, China*
[10]*School of Microelectronics and Communication Engineering, Chongqing University, Chongqing 401331, China*
[11]*College of Mathematics and Physics, Inner Mongolia Minzu University , Tongliao 028000,China*
[12]*Chengdu University of Technology，Chengdu，610059*
[13]*Shanghai Institute of Applied Physics, Chinese Academy of Sciences, Shanghai 201800, China*
[14]*Xiangtan University, Xiangtan, 411105, China*
[15]*Henan Normal University, Xinxiang, 453007, China*
[16]*Institute of Nuclear Science and Technology, Henan Academy of Sciences, Zhengzhou, 450015, China*
[17]*Fudan University, Shanghai 200433, China*
[18]*Key Laboratory of Beam Technology and Material Modification of Ministry of Education, College of Nuclear Science and Technology, Beijing Normal University, Beijing 100875, China*
[19]*Beijing Radiation Center, Beijing 100875, China*

^{147,149}Sm are slow neutron capture (s-process) nuclides in nuclear astrophysics, whose (n, γ) cross-section are the important input parameters in nucleosynthesis net calculation in the Samarium (Sm) region. Additionally, ^{149}Sm is a fission product of ^{235}U with 1% yield, and its neutron resonance parameters play a critical role in reactor neutronics. According to the available nuclear evaluation databases, significant disagreement have been observed in the resonance peaks of ^{147,149}Sm (n,γ) cross section data within the energy range of 20-300 eV. In this study, the neutron capture cross section of the natural Samarium target was measured at the back-streaming white neutron beamline of China Spallation Neutron Source. The neutron capture yield was obtained and the neutron resonance parameters for ^{147}Sm at 107.0，139.4，241.7，and 257.3 eV and ^{149}Sm at 23.2, 24.6, 26.1, 28.0, 51.5, 75.2, 90.9, 125.3, and 248.4 eV were extracted using the SAMMY code based on R-matrix theory. For the parameters Γ_n and Γ_γ in these energies of ^{147,149}Sm, the percentages consistent with the results of the CENDL-3.2, ENDF/B-VIII.0, JEFF-3.3, JENDL-4.0, and BROND-3.1 database are 27%, 65%, 65%, 42%, and 58%, respectively. Meanwhile, 27% of the results were inconsistent with them included in any of the major libraries. This work enrichis the experimental data of ^{147,149}Sm neutron capture resonance and helps to clarify the differences between different evaluation databases at the above energies.

Keywords: neutron capture cross section, neutron resonance parameters, Back-n facility

I. INTRODUCTION

The origin of super-iron elements is a current focal point in nuclear astrophysics. Over 98% of heavy elements are formed through the slow neutron capture process (s process) [1] and the fast neutron capture process (r process) [2]. However, there are stable nuclides that cannot be produced by either the s or r processes, containing more protons and separated from s and r nuclei by unstable isotopes between ^{74}Se and ^{194}Hg, collectively known as p-nuclei, with "p" representing proton-rich, totally 35 nuclei in all [3]. Despite their rarity and low abundance, the synthesis of these p-nuclei involves a wide range of nuclei. Therefore, it is crucial to investigate the mechanism of the p-process for a comprehensive understanding of nucleosynthesis. The cross-sectional and structural studies of these 35 p-nuclei provide valuable insights into the mechanism of the p-process. To gain a more precise understanding of celestial nuclear processes and related element synthesis, it is essential to study nuclear mass, reaction cross section, and decay properties [4].

Natural samarium consists of 8 stable isotopes, with ^{147,149}Sm being synthesized by the s process. Among these isotopes, ^{149}Sm is exclusively produced by the s process due to their stable neodymium isobars shielding them from con-

* Corresponding author: lixinxiang@usc.edu.cn
† Corresponding author: wanghw@sari.ac.cn
‡ Corresponding author: wenluo-ok@163.com

tributions of the r process. The (n,γ) cross section data for these isotopes can provide valuable insights into the nucleosynthesis path in the samarium region. Meanwhile, ^{235}U is an important raw material for nuclear reactors [5, 6]. As the operation of the nuclear reactor progresses, a multitude of fission product nuclides are inevitably produced from the fission of fissile materials such as ^{235}U, some of which exhibit significantly high thermal neutron absorption cross sections. Among these fission products, ^{149}Sm, with a 1% yield from ^{235}U fission, plays an important role in reactor neutronics due to its neutron capture cross section [7].

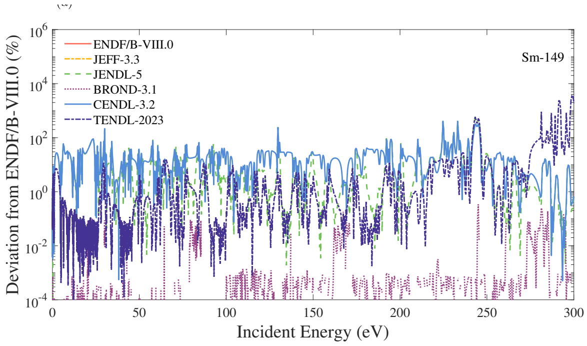

Fig. 1. (color online) the deviation in neutron capture reaction data for ^{149}Sm as reported in different evaluation databases compared to the ENDF/B-VIII.0 database.

According to the available nuclear evaluation databases such as ENDF B-VIII.0, CENDL-3.2, JENDL-4.0, JEFF-3.3, BROND-3.1, significant deviations have been observed in the resonance peaks of ^{nat}Sm (n,γ) cross section data within the energy range of 1-300 eV. Fig. 1 illustrates the deviation in neutron capture reaction data for ^{149}Sm as reported in different evaluation databases compared to the ENDF/B-VIII.0 database. The deviation is calculate by $|\sigma_i - \sigma|/\sigma$ (i=1,2,3...), where σ is the ^{149}Sm (n,γ) cross section in ENDF/B-VIII.0 database and σ_i are from the other evaluated databases. As shown in Fig. 1, in energy range between 1 and 300 eV, the cross section of ^{149}Sm (n,γ) in most evaluation databases are different from ENDF/B-VIII.0, even the deviation in database of CENDL-3.2 and JENDL-5 reaches or over 100%. As present in the available Experimental Nuclear Reaction Data (EXFOR), there is no experimental data can clarify the differences between the different evaluation databases mentioned above.

The China Spallation Neutron Source (CSNS) is a large-scale multidisciplinary application platform based on high-power proton accelerators, primarily utilized for material structure research through neutron scattering technology [8]. The CSNS accelerator comprises an 80 MeV hydrogen negative ion linear accelerator, a fast cycle proton synchrotron accelerator with an energy of 1.6 GeV, and two proton beam transport lines [9]. The provided proton beam energy at CSNS is 1.6 GeV, with a beam power of 100 kW(now in 180 kW) and a repetition frequency of 25 Hz. Tungsten targets of varying thicknesses are employed for the scattering reaction with protons, each wrapped in tantalum with a thickness of 0.5 mm and separated by cooling water layers measuring 1.5 mm thick [10, 11]. Upon impact of the proton beam on the tungsten target, the estimated neutron flux can reach 2.0×10^{16} cm^{-2}s^{-1}[12–17].

This study conducted measurements of the neutron capture cross section of natural samarium within the energy range of 20 to 300 eV at the back streaming white neutron (Back-n) facility at the CSNS [18–23]. The ^{nat}Sm experiment was concluded in 2019 and a method that integrates Monte Carlo simulation to ascertain the in-beam γ-ray background [24] was subsequently utilized in the analysis of samarium neutron capture cross section data. Resonance parameters for each isotope within this energy range were derived using SAMMY. The experimental results can clarify the difference of the ^{147,149}Sm neutron resonance parameters in different evaluation databases under specific energies. For example at the energy of 139.4 eV. The neutron resonance parameter Γ_n of ^{147}Sm isotope in the database of CENDL-3.2 and JENDL-4.0 are 69.1 meV, which is different from the database of ENDF/B-VIII.0, JEFF-3.3, and BROND-3.1 databases-the values in these databases are uniformly 88 meV. The result of this work is 89.0 ± 8.8 meV. More results and detailed analysis are presented below.

II. METHOD AND MATERIAL

A. Experimental Setup

The neutron capture experiment was conducted at the end station 2 (ES#2) of the Back-n beamline. The measurement utilized a detection system consisting of four C_6D_6 scintillation detectors, each with a diameter of 127 mm and length of 76.2 mm, housed within a 1.5-mm thick aluminum capsule and coupled with a photomultiplier tube (ETEL 930 KEB PMT). For the measurement of neutron capture reaction cross section, the C_6D_6 detector offers several advantages [25]: (1) It exhibits low sensitivity to neutrons, which is crucial for eliminating background signals in the detection of final state γ rays from the (n,γ) reaction. This insensitivity significantly reduces neutron-induced background. (2) The C_6D_6 detector demonstrates fast time response, with signal responses to neutrons and γ rays on the order of nanoseconds. Coupled with the response time of the photomultiplier tube, this results in a rise time of approximately 10 ns for the entire anode signal, thereby improving overall time resolution in detection systems. (3) Through pulse height weighting technique (PHWT), the detection efficiency of C_6D_6 detectors can be independent of decay paths, multiplicity, and energy distribution of γ rays. The physical arrangement and Monte Carlo simulation reconstruction of the detector system and target are depicted in Ref. [26], with detailed layout parameters provided in Ref .[27]. The placement of the detector is oriented opposite to the direction of the beam. This configuration effectively minimizes background interference from beam scattering, given that γ rays emitted by neutron capture reactions are isotropic. Neutron flux was determined using a Li-Si detector based on the ^{6}Li(n,α)^{3}H reaction. Energy spectra were

obtained from the Back-n collaboration, with an uncertainty of less than 8.0% for $E_n < 0.15$ MeV [28]. The Back-n data acquisition system (DAQ) employs a full waveform data acquisition solution.

In this study, the TOF (time of flight) method was used to determine the resonance energy of neutrons. The E_n can expressed as follow:

$$E_n = \frac{1}{2} m_n (\frac{L}{t_n})^2, \quad (1)$$

where m_n is the neutron mass, L is the flight distance, and t_n is the flight time. At Back-n facility, t_n is determined as $t_n = (t_{det} - t_\gamma) + \frac{L}{c}$, where t_{det} denotes the time when the detector responds to neutrons or γ rays; t_γ is the time when the γ-flash arrives at the detector, c is the speed of light [29]. The ES#2 is about 76 m away from the spallation target, and the value of L is 77.26 m in our case. The uncertainty of L is mainly caused by the multiple scattering of neutrons inside the spallation target [30].

In the normal operation mode of CSNS there are two proton bunches with a time interval of 410 ns in each pulse which has a repetition frequency of 25 Hz. Due to the superposition of the event distributions corresponding to two bunches, the resolution of the TOF measurement at Back-n will be degraded by the double-bunch characteristics if the measured event distribution is used directly without unfolding, especially in the higher neutron energy region [31]. In this work, we use the analytical method developed by the Back-n collaboration to nearly recover the event distribution corresponding to a single proton bunch [32].

The experiment was conducted in May 2019, involving the preparation of a gold (^{197}Au) target, a carbon ($^{\text{nat}}$C) target, an empty target, and a natural samarium ($^{\text{nat}}$Sm) target. A total beam time of approximately 49 hours was allocated for the study. The ^{197}Au(n,γ)^{198}Au reaction, serving as a standard neutron capture cross section, was initially measured for 13 hours at proton power levels ranging from 50.5 to 51.9 kW to validate previous findings [26], thereby ensuring the integrity of the experimental setup and data acquisition(DAQ) system. Subsequently, measurements were carried out on the carbon and empty targets for 12 and 8 hours respectively to assess neutron scattering background and environmental interference under beam conditions. Throughout this period, the accelerator exhibited relatively stable performance with a beam power of approximately 50 kW and an uncertainty level below 2%. Finally, the natural samarium target underwent measurement for 16 hours at beam power levels between 48.3 and 50.5 kW. Details regarding target parameters and measurement conditions are presented in Table 1, with diameter measurements obtained using vernier calipers and thickness determined by micrometer readings.

B. Weighting Function

The essence of the data analysis lies in obtaining the counts of neutron capture reactions within the target, a process contingent upon the detection efficiency and accuracy of the detector's response to (n, γ) reactions. The efficacy of C_6D_6 scintillators in detecting prompt γ-ray cascades emitted during neutron capture reactions is contingent upon the intricate de-excitation path of the compound nucleus. As a result, it is imperative that the measured signals undergo pulse height weighting technique (PHWT), which serves to render detection efficiency independent of cascade γ-ray energies.

Typically, a high detection efficiency is sought after; however, for neutron capture reactions, a low detection efficiency is preferred due to the phenomenon of γ radiation cascade emission. In the case of a neutron capture cascade emission, it is desirable to detect at most one γ ray in the cascade emission, making low detection efficiency more suitable. Therefore, the detection efficiency for the capture reaction is approximately equal to the sum of the detection efficiencies for the capture reaction cascade γ.

$$\varepsilon_c = 1 - \prod(1 - \varepsilon_{\gamma i}) \approx \sum \varepsilon_{\gamma i}, \quad (2)$$

where ε_c is the detection efficiency of C_6D_6 detector for capture reaction; $\varepsilon_{\gamma i}$ is the detection efficiency of the i^{th} cascade γ ray; Since $\varepsilon_{\gamma i}$ is small enough, the equal sign of the above formula holds. Equation (2) establishes the relationship between ε_c and $\varepsilon_{\gamma i}$, but it cannot be directly reflected in the output energy spectrum of C_6D_6 detector. We hope to establish a direct relationship between ε_c and the output energy spectrum of the detector, which is helpful to directly analyze ε_c from the output signal of the detector, and then calculate the neutron capture cross section. If the γ detection efficiency in equation (2) is proportional to the γ energy E_γ, i.e.:

$$\varepsilon_{\gamma i} = \alpha E_{\gamma i}. \quad (3)$$

Then,

$$\varepsilon_c = \alpha \sum E_{\gamma i}, \quad (4)$$

where α is the scale coefficient, and E_γ is the energy of the cascade γ, which can be obtained directly from the pulse height spectrum output by C_6D_6.

In order for equation (4) to hold, it is necessary to perform mathematical control on the response function of the detection system to realize the relation of (3), which is Pulse Height Weighting Techniques (PHWT). The PHWT was first proposed by Macklin and Gibbons and applied to the C_6F_6 detector to measure the neutron capture cross section [33]. We anticipate that the energy of each group of cascaded γ-rays will be directly proportional to the weighted detection efficiency. The normalized detection efficiency will manifest intuitively in the pulse height spectrum (PH spectrum) counts. Consequently, the detector's detection efficiency towards γ can be effectively characterized by analyzing the pulse height spectrum. By introducing a weighted function Number, we ensure that the following equation is satisfied.

$$\int_{EL}^{\infty} R_d(E_d, E_{\gamma j}) W(E_d) d(E_d) = \alpha E_{\gamma j}, \quad (5)$$

Table 1. Information of experimental targets

Target	Impurities			Diameter (mm)	Thickness (mm)	Beam Power (kW)
^{nat}Sm	$\omega(\mathrm{Mo}) = 0.002\%$	$\omega(\mathrm{Ti}) = 0.002\%$	$\omega(\mathrm{Tb}) = 0.001\%$	50.00 ± 0.02	1.000 ± 0.005	49.37 ± 1.08
	$\omega(\mathrm{Fe}) = 0.01\%$	$\omega(\mathrm{Ca}) = 0.005\%$	$\omega(\mathrm{C}) = 0.01\%$			
	$\omega(\mathrm{Si}) = 0.01\%$	$\omega(\mathrm{Mg}) = 0.005\%$	$\omega(\mathrm{Nb}) = 0.002\%$			
	$\omega(\mathrm{Al}) = 0.005\%$	$\omega(\mathrm{Cl}) = 0.005\%$	$\omega(\mathrm{Ta}) = 0.002\%$			
	$\omega(\mathrm{La}) = 0.001\%$	$\omega(\mathrm{Ce}) = 0.001\%$	$\omega(\mathrm{Pr}) = 0.002\%$			
^{nat}C	$< 0.100\%$			50.00 ± 0.02	1.000 ± 0.005	50.00 ± 1.00
^{197}Au	$< 0.100\%$			30.00 ± 0.02	1.000 ± 0.005	51.20 ± 0.70

where the EL is the threshold of PH spectrum; E_d is an energy bin of PH spectrum; $R(E_d, E_{\gamma j})$ is counts of PH spectrum with energy response function in E_d; $W(E_d)$ is the weight factor corresponding to E_d; $E_{\gamma j}$ is the energy of gamma-ray of group j, here we set the coefficient $\alpha = 1$.

Experimental capture yields were determined using a weighting function (WF) parameterized as polynomial functions of the γ-ray energy. WF can be expressed as

$$WF(E_d) = \sum_{i=0}^{4} a_i E_d^i, \tag{6}$$

where a_i is the parameters of the WF, and it can be determined by least squares method fit:

$$\chi^2 = \sum (kE_{\gamma j} - \int_{EL}^{\infty} R(E_d, E_{\gamma j}) WF(E_d) dE_d)^2. \tag{7}$$

Each event is weighted by the appropriate WF to ensure that the detector's weighted efficiency is directly proportional to their excitation energy, as illustrated in Fig. 2. This manipulation of raw data remains valid when the original efficiency is sufficiently low, allowing for the measurement of only one γ ray per capture event in the C_6D_6 setup [34].

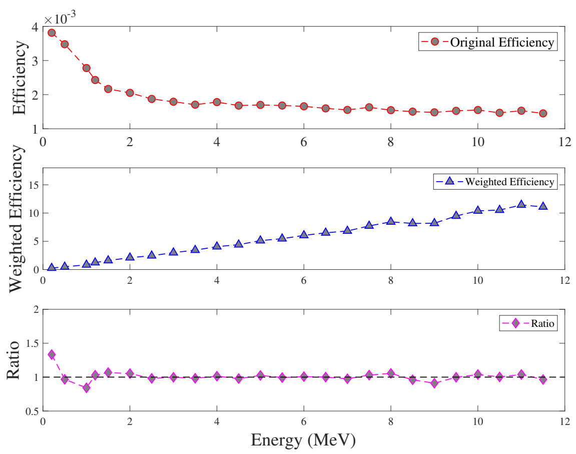

Fig. 2. (color online) (a) The C_6D_6 original efficiency. (b) Weighted efficiency. (c) The ratio of weighted efficiency to γ rays energy.

The energy deposition of different mono-energetic γ rays in the C_6D_6 detector layout [24] was simulated using the Geant4 Monte Carlo program [35, 36]. The original efficiency curve is presented in Fig. 2(a). Upon application of the weight function to the original efficiency curve, a linear relationship between detection efficiency and energy is illustrated in Fig. 2(b), with the ratio of efficiency to energy in Fig. 2(c) approaching unity. Below 1.5 MeV, the weighted efficiency does not exhibit proportionality to energy, necessitating the establishment of a threshold during PH spectrum processing to mitigate any impact from the weight function's failure.

C. Background Analysis

The WF needs to be applied on the net pulse height spectrum to be effective. The key to obtaining a net pulse height spectrum is the deduction of background. For neutron capture cross section measurements with C_6D_6 detectors at Back-n, the background composition is as follows [37]:

$$B(t) = B_0 + B_{empty}(t) + B_{sample}(t), \tag{8}$$

where B_0 is sample- and time- independent background; $B_{empty}(t)$ is the background that is time dependent but sample independent; $B_{sample}(t)$ is the sample dependent background, which is related to the scattering of neutrons and γ-rays by the sample. The neutron energy E_n is derived from the time of flight t, therefore,

$$B(E_n) = B_0 + B_{empty}(E_n) + B_{sn}(E_n) + B_{s\gamma}(E_n), \tag{9}$$

where B is the total background which is related to the neutron energy E_n; B_{sn} is the background caused by neutron scattering with the target and $B_{s\gamma}$ is the background caused by in-beam γ scattering with the target.

The background resulting from environmental activation and delayed γ rays is independent of the sample and time, but solely relies on the experimental conditions. The background in this context is determined by measuring an empty target without a beam to establish B_0. On the other hand, the background arising from both the beam and the environment is not influenced by the sample, but does vary with time. This aspect of the background is assessed by measuring an empty target under beam conditions to determine $B_{empty}(E_n)$.

The background caused by neutron scattering typically necessitates a target nucleus with a large neutron scattering

cross section in the relevant energy range, while also requiring the neutron capture cross section of the target nucleus to be relatively flat so as not to interfere with the measurement of the Sm target. In this study, we utilized measurements of the carbon target under beam conditions to determine $B_{sn}(E_n)$. Given its low neutron capture cross section compared to Sm and absence of resonance structure in the relevant energy range, lead is an ideal material for evaluating in-beam γ background $B_{s\gamma}(E_n)$ since its strong γ ray scattering capability.

In 2019, we failed to recognize the significance of in-beam γ background and consequently overlooked this aspect of the data. However, in 2022, we were able to ascertain the general time structure of in-beam γ background at the Back-n facility through various in-beam γ ray experimental findings [24]. Subsequently, we proposed a methodology for comprehensive quantification of in-beam γ rays based on Geant4 simulation. By re-analyzing the 2019 ^{nat}Er target experimental results using this approach, we obtained reliable outcomes that validated its efficacy. Furthermore, employing this method, we also processed the 2019 ^{nat}Sm target experimental data to determine $B_{s\gamma}(E_n)$.

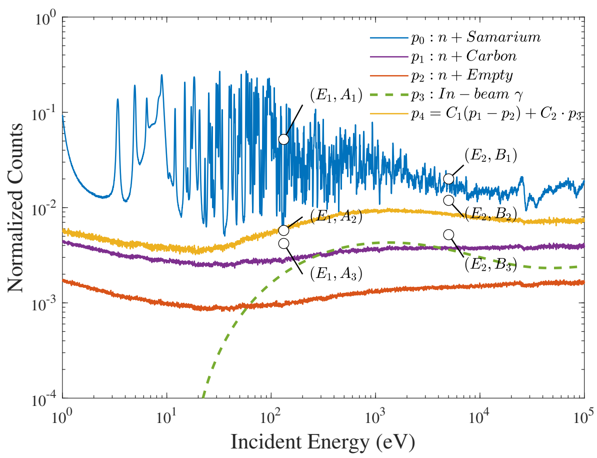

Fig. 3. (color online) The spectrum of natural samarium target, empty target and carbon target (normalized to the neutron flux rate), the in-beam γ ray background is determined by simulation, as the method provided in Ref. [24]

The normalized counts spectrum is presented in Fig. 3. The lines $p_0 - p_2$ represent the spectra of natural samarium target, carbon target, and empty target, which are normalized to the neutron flux rate detected by a Li-Si detector. Line p_3 corresponds to the in-beam γ ray background, with its shape measured using a lead target. As discussed in Ref.[24], there exists a general formula and parameters for expressing its shape at the Back-n facility until significant modifications are made to the beamline that may impact the generation or transportation of in-beam γ rays. We consider the inclusion of a Co filter at the beamline, which exhibits two distinct resonance absorption peaks at energies of $E_1 = 132$ eV and $E_2 = 5.016$ keV. When the thickness of the filter is designed to completely absorb neutrons, only γ rays remain in the beam. Consequently, $A_1(B_1)$ corresponds to line p_0 at an energy of $E_1(E_2)$, representing the result of natural samarium reacting with neutrons and γ rays; while $A_2(B_2)$ is obtained through simulation, depicting the outcome of natural samarium target interacting solely with γ rays.

Let $A_3 = A_2\sigma_1/\sigma_2(B_3 = B_2\sigma_1/\sigma_2)$, where $\sigma_1(\sigma_2)$ is the γ-ray elastic cross section of lead and ^{nat}Sm target. $p_4 = C_1(p_1 - p_2) + C_2 \cdot p_3$. C_1 is the ratio of neutron scatering cross section of samarium to carbon. Let the point (E_1, A_3) and (E_2, B_3) in the line p_4, the parameter C_2 can be determined.

III. RESULTS AND DISCUSSION

A. Neutron Capture Yield

The net PH spectrum is derived by subtracting the background. Following the application of WFs, the capture yield can be determined as follows:

$$Y_w(E_n) = \frac{N_w(E_n)}{N_s I(E_n) S_n}, \tag{10}$$

where $Y_w(E_n)$ is the capture yield, $N_w(E_n)$ is the weighted pulse height spectrum, N_s is the target area density, $I(E_n)$ is the neutron flux measured by Back-n collaboration [28], S_n is the target neutron separation energy. For the natural Sm target, each individual resonance corresponds to a specific isotope and possesses its own separation energy for capture efficiency. Consequently, the value of S_n varies across different resonance peaks. The method for calculating the value of S_n for the ^{nat}Sm target is illustrated in Fig. 4. Different colors stand for different isotopes of Sm element. Line types (including dot lines, solid lines, and dashed lines) indicate the variations of neutron capture cross sections of isotopes with incident neutron energy, and dot types represent the different values of neutron separation energy S_n. Both linear and point patterns are presented in Figure 4 to demonstrate that the value of natural target S_n is based on the contribution of different isotopes to the resonance peaks. Since S_n ranges from 5.81 MeV (^{154}Sm) to 8.15 MeV (^{147}Sm), no significant difference can be observed on the y axis scale of Fig. 4, and $S_n \times max(\sigma)$ is employed to reflect the value of natural target S_n at different energies. As the dot styles in Fig. 4 shows, since different isotopes contribute different resonance peaks, the S_n value of the natural target is a piecewise function, which is related to the formant position of different isotopes. The values of S_n for ^{nat}Sm isotopes can be obtained according to the new atomic mass evaluation (AME2020) [38].

B. Uncertainty

The uncertainty in the capture yield encompasses several contributing factors, as outlined in [27]: variability arising from experimental conditions, data analysis, and statistical error.

The uncertainty arising from experimental conditions encompasses variations in the energy spectrum and proton beam

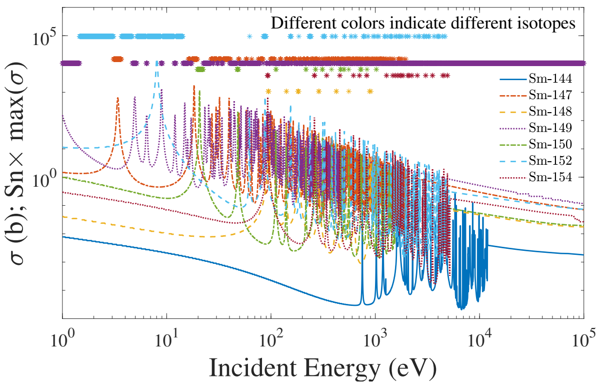

Fig. 4. (color online) The normalized value of cross section for different isotopes and the value of S_n for natural samarium element. Line types (including dot lines, solid lines, and dashed lines) indicate the variations of neutron capture cross sections of nuclides with incident neutron energy, and dot types represent the values of natural S_n at different energies.

power, both of which directly impact the neutron flux at the target. This uncertainty is subsequently propagated into the yield through the term of I in Eq.(9). According to findings from the Back-n collaboration [28], the uncertainty associated with the energy spectrum in Back-n ES#2 without a lead absorber ranges between 2.3% and 4.5% above 0.15 MeV, and less than 8.0% below 0.15 MeV. The uncertainties stemming from beam power are detailed in table 1. As shown in table 1, apart from the Sm element, the target material also contains trace quantities of other elements, and their contents vary from 0.001% to 0.01%. As the contents of these impurities are sufficiently low, their impact on the measurement results of the Sm neutron capture cross section is less than 1%.

The uncertainties in data analysis are primarily attributed to the PHWT method. In a study by Tain et al. in 2002, the neutron width PHWT treatment results of a 1.15 keV peak in ^{56}Fe were compared with experimental results, revealing a systematic error of 2.00%–3.00% [39]. This level of uncertainty can only be achieved if proper consideration is given to threshold, conversion electron, and γ-ray summing effects. Our simulation involved a complete reconstruction of the target system and detector system, while also incorporating a cascade γ emission program that includes a model of internal conversion processes. These efforts serve to minimize additional uncertainty when applying PHWT to our results.

On the contrary, the uncertainty stemming from the normalization method used to determine the absolute value of the term of I in Eq. (9) will also impact the precision of capture yield. Two normalization methods were provided in Ref. [27]: Gaussian fitting of one of the resonance peaks (typically selecting the first peak in the experimental energy region, which for a $^{\rm nat}$Sm target is at 3.4 eV). The normalized coefficient is calculated by comparing the fitted curve with evaluation data, and CENDL-3.2 database was utilized in this study. Another approach involves comparing energy bins individually. The normalized uncertainty varies for different targets, and for $^{\rm nat}$Sm, it is less than 1.3%.

The $^{\rm nat}$Sm experiment was concluded in 2019, and the experimental data for in-beam γ-ray background was unfortunately not obtained. As a result, we have employed the methodology outlined in Ref. [37] to analyze the in-beam γ-ray background. The uncertainty within the energy range of 20 to 300 eV is found to be less than 10.5%.

Finally, the statistical uncertainty of the experiment was smaller than 0.68%. All error sources and their estimates are summarized in Table 2.

C. Neutron Resonance Parameters

The neutron capture yield of a natural samarium target was measured within the resonance energy range of 1-300 eV. The capture yield data was obtained using Eq. 10 and subsequently fitted using the R-Matrix code SAMMY, accounting for various experimental effects such as Doppler broadening, self-shielding, and multiple scattering. The resonance parameters of $^{\rm nat}$Sm(n,γ) were then extracted accordingly. The fitting result is also depicted in Fig. 5. In the resonance energy region, each peak is contributed by a specific nuclide. Thus, the resonance information of each isotope can be extracted from the results of natural targets based on the resonance energy. Furthermore, Table 3 presents a detailed comparison of differences between different evaluation databases (DB#1-5 representing CENDL-3.2, ENDF/B-VIII.0, JEFF-3.3, JENDL-4.0, BROND-3.1).

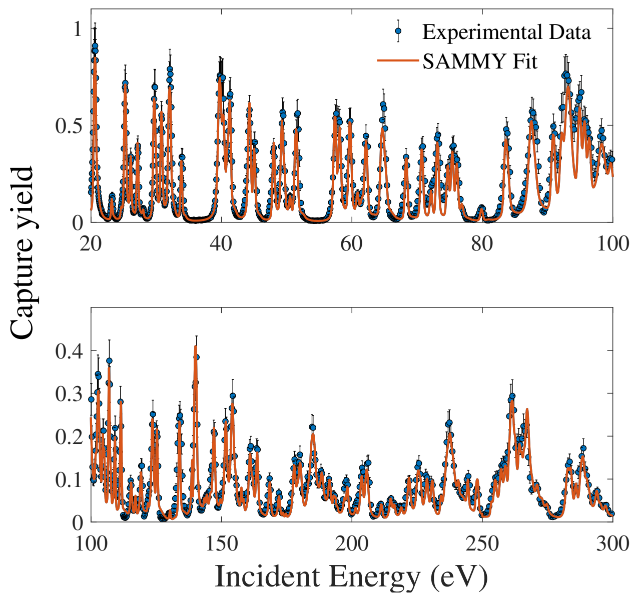

Fig. 5. (color online) The experimental capture yields and the fitted ones obtained with the SAMMY code.

The comparison of the current study's findings with those from various evaluation libraries is illustrated in Fig. 6

Table 2. The statistical error and systematic error of the experiment

σ	Meaning	Value
	Experimental Conditions	
$\sigma(BeamPower)$	Uncertainty from beam power	see Table 1
$\sigma(Target)$	Uncertainty from impurities in the target	$< 1\%$
$\sigma(I_2)$	Uncertainty from energy spectra below 0.15 MeV	$< 8.00\%$
	Data Analysis	
$\sigma(PHWT)$	Uncertainty from PHWT method	$< 3.00\%$
$\sigma(Normalized)$	Uncertainty from normalized	$< 1.30\%$
$\sigma(In-Beam)$	Uncertainty from counts of in-beam BKG	$< 10.5\%$
	Statistical error	
$\sigma(Statistic)$	Uncertainty from mathematical statistics	$< 0.68\%$

(^{147}Sm) and Fig. 7 (^{149}Sm). For the ^{147}Sm isotope, the parameter Γ_n remains consistent at 107.0 eV across different evaluation databases, and our experimental results are in agreement with all of them. However, at energy points of 139.4 eV, 241.7 eV, and 257.3 eV, the parameter Γ_n in the CENDL-3.2 database aligns with the JENDL-4.0 database but diverges from the ENDF/B-VIII.0, JEFF-3.3, and BROND-3.1 databases. For these energy points, our experimental results are consistent with the evaluations in the ENDF/B-VIII.0, JEFF-3.3, and BROND-3.1 databases. The value of parameter Γ_γ for ^{147}Sm in the CENDL-3.2 database is 69 meV at 107 eV compared to 82 meV in the other four databases; however, our present experimental result is 85.5 ± 8.0 meV.

For the ^{149}Sm isotope, the discrepancy in the parameter Γ_n across different evaluation databases is minimal, and the experimental findings align closely with the assessment databases at most energy levels. Specifically, our present experiment yields a value of 25.8 ± 2.5 meV at an energy of 248.4 eV, whereas four evaluation databases report values ranging from 36.6 to 39.7 meV. The Γ_γ value in the CENDL-3.2 database aligns with that of the JENDL-4.0 database at energy points such as 23.2, 24.6, 26.1, and 28.0 eV. However, it diverges from the evaluation databases of ENDF/B-VIII.0, JEFF-3.3, and BROND-3.1. At energy points of 51.5, 75.2, 90.9, 125.3 and 248.4 eV., the experimental results are consistent with those in the ENDF/B-VIII.0, JEFF-3.0, JENDL-4.0, and BROND-3.1 databases.

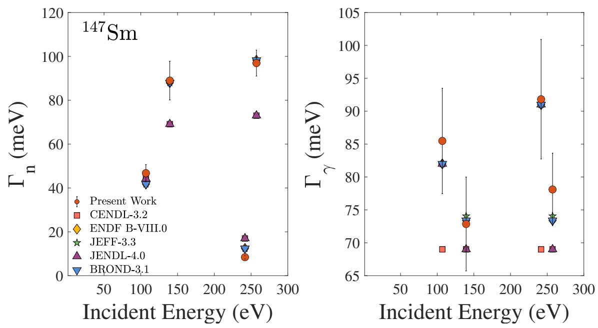

Fig. 6. (color online) Comparison between the Γ_n and Γ_γ values of ^{147}Sm obtained from the different databases and this work.

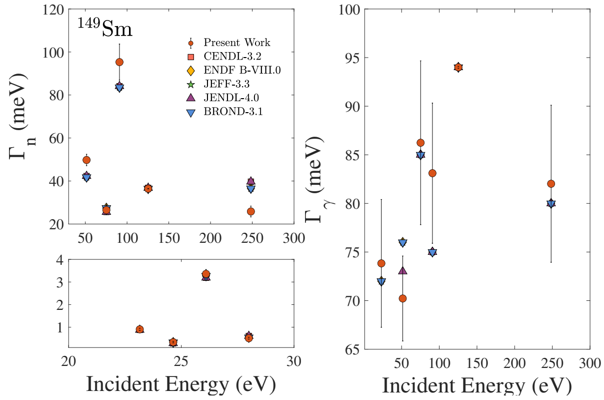

Fig. 7. (color online) Comparison between the Γ_n and Γ_γ values of ^{149}Sm obtained from the different databases and this work.

IV. SUMMARY AND CONCLUSIONS

The neutron capture cross section of a natural samarium target was measured at the Back-n facility in China spallation neutron source. Environmental background and neutron scattering background were subtracted through experimental measurement, while in-beam γ-ray background was removed by combining experiment and simulation. Subsequently, the neutron resonance parameters for various isotopes of Sm from 20 to 300 eV were extracted using the SAMMY code based on R-matrix theory. For the parameters Γ_n and Γ_γ in these energies of ^{147,149}Sm, the percentages consistent with the results of the CENDL-3.2, ENDF/B-VIII.0, JEFF-3.3, JENDL-4.0, and BROND-3.1 database are 27%, 65%, 65%, 42%, and 58%, respectively. Meanwhile, 27% of the results were inconsistent with them included in any of the major libraries. This work enrichis the experimental data of ^{147,149}Sm neutron capture resonance and helps to clarify the differences between different evaluation databases at the above energies.

Table 3. Clarification of differences between different evaluation databases

Mass	E_n (eV)	Γ_n						Γ_γ					
		Present Work	DB#1	DB#2	DB#3	DB#4	DB#5	Prensent Work	DB#1	DB#2	DB#3	DB#4	DB#5
147	107.0	46.8 ± 4.0	44.2	41.8	41.8	44.2	41.8	85.5 ± 8.0	69.0	82.0	82.0	82.0	82.0
	139.4	89.0 ± 8.8	69.1	88.0	88.0	69.1	88.0	72.9 ± 7.1	69.0	73.4	74.1	69.0	73.4
	241.7	8.4 ± 0.8	17.0	12.4	12.4	17.0	12.4	91.8 ± 9.2	69.0	91.0	91.0	91.0	91.0
	257.3	96.9 ± 6.5	73.0	98.3	98.3	73.0	98.3	78.1 ± 5.8	69.0	73.4	74.1	69.0	73.4
149	23.2	0.9 ± 0.1	0.9	7.9	7.9	0.9	7.9	73.8 ± 6.8	62.0	72.0	72.0	62.0	72.0
	24.6	0.3 ± 0.1	0.3	0.3	0.3	0.3	0.3	39.4 ± 3.9	62.0	40.0	40.0	62.0	40.0
	26.1	3.4 ± 0.3	3.2	3.3	3.3	3.2	3.3	51.7 ± 5.0	62.0	49.0	49.0	62.0	49.0
	28.0	0.5 ± 0.1	0.6	0.5	0.5	0.6	0.5	39.7 ± 4.0	62.0	40.0	40.0	62.0	40.0
	51.5	49.8 ± 3.2	42.3	41.8	41.8	42.3	41.8	70.2 ± 5.1	62.0	76.0	76.0	73.0	76.0
	75.2	26.5 ± 2.3	25.6	27.4	27.4	25.6	27.4	86.2 ± 8.4	62.0	85.0	85.0	85.0	85.0
	90.9	95.3 ± 8.8	84.1	83.6	83.6	84.1	83.6	83.1 ± 7.2	62.0	75.0	75.0	75.0	75.0
	125.3	36.4 ± 4.0	36.8	36.4	36.4	36.8	36.4	94.0 ± 9.8	62.0	94.0	94.0	94.0	94.0
	248.4	25.8 ± 2.6	39.7	36.6	36.6	39.7	36.6	82.0 ± 8.1	62.0	80.0	80.0	80.0	80.0

ACKNOWLEDGMENTS

We appreciate effective technical support from Dr. Yi-Jie Wang at Tsinghua University, Dr. Yu-Chao Xu at General Electric, Dr. Xing-Yuan Xu at University of Science and Technology of China and the efforts of the CSNS and Back-n staff. We Also thank Hunan WeiYu network Technology Co., Ltd. to provide technical support.

This work was supported by the National Key Research and Development Program (Grant No.2022YFA1603300) and National Natural Science Foundation of China (No.12275338, No.12388102). China Institute of Atomic Energy(No.CIAE-FW-GKJT-23-0820).

[1] Käppeler F, Gallino R, Bisterzo S, The s process: Nuclear physics, stellar models, and observations. Rev. Mod. Phys. **83** 157-193 (2011). doi: 10.1103/RevModPhys.83.157

[2] Cowan, John J and Thielemann, Friedrich-Karl, The r-process and nucleochronology. Phys. Rep. **208**, 267-394 (1991). doi: 10.1016/0370-1573(91)90070-3

[3] Arnould, M and Goriely, S, The p-process of stellar nucleosynthesis: astrophysics and nuclear physics status. Phys. Rep. **384** 1-84 (2003). doi: 10.1016/S0370-1573(03)00242-4

[4] Penionzhkevich, Yu E, Nuclear astrophysics. Phys. Atom. Nucl. **73** 1460-1468 (2010). doi: 10.1134/S106377881008020X

[5] Tan C X, Li X X, Pang D Y, et al., ^{233}Pa (n,γ) cross section extraction using the surrogate reaction ^{232}Th(^{3}He, p)^{234}Pa* involving spin-parity distribution. Phys. Rev. C. **109** 044615 (2024). doi: 10.1103/PhysRevC.109.044615

[6] Wang K, Wang X D and Fei X H, et al., Evaluation of polycarbonate films as detection materials for high dose electron beam radiation detection. Accepted by Nucl. Sci. Tech.

[7] Xiong H H, Zeng Q S, Han Y C, et al., Neutronics analysis of a subcritical blanket system driven by a gas dynamic trap-based fusion neutron source for ^{99}Mo production. Nucl. Sci. Tech. **34**, 49 (2023). doi: 10.1007/s41365-023-01206-2

[8] Chen H, Wang X L, China's first pulsed neutron source. Nature materials. **15**, 689–691 (2016). doi: 10.1038/nmat4655

[9] Jiang B, Tian B B, Jing H T,et al., Feasibility of medical radioisotope production based on the proton beams at China Spallation Neutron Source. Nucl. Sci. Tech. **35**, 102 (2024). doi: 10.1007/s41365-024-01438-w

[10] Xue J, Feng S, Chen Y, Measurement and analysis of the neutron-induced total cross-sections of ^{209}Bi from 0.3 eV to 20 MeV on the Back-n at CSNS. Chin. Phys. C. **47**, 124001 (2023). doi: 10.1088/1674-1137/acf920

[11] Yang G L, An Z D, Jiang W, Measurement of Br(n, γ) cross sections up to stellar s-process temperatures at the CSNS Back-n. Nucl. Sci. Tech. **34**, 180 (2023). doi: 10.1007/s41365-023-01337-6

[12] Wang S, Fang S X, Fu S N, et al., Introduction to the overall physics design of CSNS accelerators. Chin. Phys. C. **33**, 1(2009). doi: 10.1088/1674-1137/33/S2/001

[13] Wang S, An Y W, Fang S X, An overview of design for CSNS/RCS and beam transport. Sci. China. Ser. G. **54**, 239–244 (2011). doi: 10.1007/s11433-011-4564-x

[14] Liang T R, Li Z D, Yin W, et al., Simulation of a high energy neutron irradiation facility at beamline 11 of the China spallation neutron source. Nucl. Instrum. Meth. A. **860** 24-28 (2017). doi: 10.1016/j.nima.2017.04.004

[15] Liu H, Peng J, Gong K, et al. The design and construction of CSNS drift tube linac. Nucl. Instrum. Meth. A. **911** 131-137 (2018). doi: 10.1016/j.nima.2018.10.034

[16] Zhu L, Zhou J R, Xia Y G, et al., Large area ^{3}He tube array detector with modular design for multi-physics instrument at CSNS. Nucl. Sci. Tech. **34** 1 (2023). 10.1007/s41365-022-01161-4

[17] Li Q, Luan G Y, Bao J, et al., The ^{6}LiF-silicon detector array developed for real-time neutron monitoring at white neutron beam at CSNS. Nucl. Instrum. Meth. A. **946** 162497 (2019).10.1016/j.nima.2019.162497

[18] Fan R, Jiang H, Jiang W, et al., Detection of low-energy charged-particle using the ΔE-E telescope at the Back-n white neutron source. Nucl. Instrum. Meth. A. **981** 164343 (2020). doi: 10.1016/j.nima.2020.164343

[19] Zhang S, Li G, Jiang W, et al., Measurement of the ^{159}Tb(n, γ) cross section at the CSNS Back-n facility. Phys. Rev. C. **107**

045809 (2023). doi: 10.1103/PhysRevC.107.045809

[20] Jiang H Y, Jiang W, Cui Z, et al., Measurement of the relative differential cross sections of the ^{1}H (n,el) reaction in the neutron energy range from 6 MeV to 52 MeV. Eur. Phys. J. A. **57** 1-18 (2021). doi: 10.1140/epja/s10050-020-00313-7

[21] Zhao D J, Feng S, Cheng P J, Conceptual design of a $Cs_2LiLaBr_6$ scintillator-based neutron total cross section spectrometer on the Back-n beam line at CSNS. Nucl. Sci. Tech. **34**, 3 (2023). doi: 10.1007/s41365-022-01152-5

[22] Tang J Y, An Q, Bai J B, Back-n white neutron source at CSNS and its applications. Nucl. Sci. Tech. **32**, 1–10 (2021). doi: 10.1007/s41365-021-00846-6

[23] Fan R R, Li Q, Bao J, et al., Detector development at the Back-n white neutron source. Radiation Detection Technology and Methods. **7**, 171–191 (2023). doi: 10.1007/s41605-022-00379-5

[24] Li X X, Liu L X, Jiang W, et al., Experimental determination of the neutron resonance peak of ^{162}Er at 67.8 eV. Phys. Rev. C. **106**, 065804 (2022). doi: 10.1103/PhysRevC.106.065804

[25] Ren J, Ruan X, Bao J, The C_6D_6 detector system on the Back-n beam line of CSNS. Radiation Detection Technology and Methods. **3**, 1–9 (2019). doi: 10.1007/s41605-019-0129-8

[26] Hu X R, Fan G T, Jiang W, et al., Measurements of the ^{197}Au(n, γ) cross section up to 100 keV at the CSNS Back-n facility. Nucl. Sci. Tech. **32**, 101 (2021). doi: 10.1007/s41365-021-00931-w

[27] Li X X, Liu L X, Jiang W, et al., New experimental measurement of ^{nat}Er(n, γ) cross sections between 1 and 100 eV. Phys. Rev. C. **104**, 054302 (2021). doi: 10.1103/PhysRevC.104.054302

[28] Chen Y, Luan G Y, Bao J, Neutron energy spectrum measurement of the Back-n white neutron source at CSNS. Eur. Phys. J. A. **55**, 1–10 (2019). doi: 10.1140/epja/i2019-12808-1

[29] Wang J C, Ren J, Jiang W, et al., In-beam gamma rays of CSNS Back-n characterized by black resonance filter. Nucl. Sci. Tech. **35**, 164 (2024). doi.org/10.1007/s41365-024-01553-8

[30] Jiang B, Han J l, Jiang W, et al., Monte-Carlo calculations of the energy resolution function with Geant4 for analyzing the neutron capture cross section of ^{232}Th measured at CSNS Back-n. Nucl. Instrum. Meth. A. **1013**, 165677 (2021). doi: 10.1016/j.nima.2021.165677

[31] Liu X Y, Yang Y W, Liu R, et al., Measurement of the neutron total cross section of carbon at the Back-n white neutron beam of CSNS. Nucl. Sci. Tech. **30**, 139 (2019). doi: 10.1007/s41365-019-0660-9

[32] Yi H, Wang T F, Li Y, et al. Double-bunch unfolding methods for the Back-n white neutron source at CSNS. J. Instrum. **15**, 03 (2020). doi: 10.1088/1748-0221/15/03/P03026

[33] Macklin R L, Gibbons J H, ^{208}Pb(n, γ) Cross Sections by Activation between 10 and 200 keV. Phys. Rev. **181**, 1639 (1969). doi: 10.1103/PhysRev.181.1639

[34] Jiang B, Han J L, Ren J, et al., Measurement of ^{232}Th(n, γ) cross section at the CSNS Back-n facility in the unresolved resonance region from 4 keV to 100 keV. Chin. Phys. B. **31**, 060101 (2022). doi: 10.1088/1674-1056/ac5394

[35] Agostinelli S, Allison J, Amako K, GEANT4—a simulation toolkit. Nucl. Instrum. Meth. A. **506**, 250–303 (2003). doi: 10.1016/S0168-9002(03)01368-8

[36] Shi X M, Wang G L, Luo K J, et al., Geant4 development for actinides photofission simulation. Nucl. Instrum. Meth. A. **1062** 169222 (2024). doi: 10.1016/j.nima.2024.169222

[37] Li X X, Liu L X, Jiang W, et al., Measurements of the ^{107}Ag neutron capture cross sections with pulse height weighting technique at the CSNS Back-n facility. Chin. Phys. B. **31**, 038204 (2022). doi: 10.1088/1674-1056/ac48fd

[38] Huang W J, Wang M, Kondev F G, The AME 2020 atomic mass evaluation (I). Evaluation of input data, and adjustment procedures. Chin. Phys. C. **45**, 030002 (2021). doi: 10.1088/1674-1137/abddb0

[39] Tain J L, Gunsing F, Aniel-Cano D, Accuracy of the pulse height weighting technique for capture cross section measurements. J. Nucl. Sci. Technol. **39**, 689–692 (2002). doi: 10.1080/00223131.2002.10875193